# Approximations for Nonequilibrium Hypervelocity Aerodynamics

R. J. Stalker*
*University of Queensland, Brisbane, Australia*

**The exponential term in the expression for the forward reaction rate in a nonequilibrium dissociating gas has been exploited to produce three simplified, approximate concepts that assist in understanding the effects of nonequilibrium in hypervelocity flows. The concepts are as follows: a constant-temperature approximation, the thermodynamic decoupling of the temperature, and pressure-gradient reaction quenching. These concepts are seen to allow satisfactory prediction of shock standoff on a sphere, the growth of shock detachment on a wedge, the variation of shock standoff on a delta wing, and the shock-layer density profile downstream of a curved shock. The mechanism underlying the constant-temperature approximation also makes it possible to develop a second-order theory of nearly constant-pressure flows, which is used to predict the nonequilibrium center-of-pressure shift on wedges and delta wings**

## Nomenclature

| | |
|---|---|
| $a$ | = sphere radius |
| $B$ | = crossflow velocity factor |
| $C$ | = reaction constant, Eq. (1) |
| $D$ | = dissociation energy per unit mass |
| $h$ | = enthalpy per unit mass |
| $K$ | = reaction constant (density) |
| $\ell$ | = chord length |
| $\Delta M$ | = pitching moment |
| $n$ | = pre-exponential temperature index |
| $p$ | = pressure |
| $\Delta p_n$ | = pressure change after plane or conical shock |
| $\Delta p_t$ | = shock shape change—induced pressure |
| $\Delta p$ | = reaction-induced surface pressure change |
| $q$ | = velocity along streamline |
| $r$ | = nose radius |
| $R$ | = shock radius of curvature |
| $s$ | = distance from shock along streamlines |
| $T$ | = reduced temperature $= \Theta_d^{-1} x$ actual temperature |
| $T_Q$ | = reduced quench temperature |
| $u_\infty$ | = mainstream velocity |
| $w$ | = wedge face length; spanwise velocity |
| $x$ | = distance from leading edge |
| $\Delta x$ | = distance for wave reflection cycle |
| $x,z,\eta$ | = conical coordinates |
| $y$ | = coordinate normal to reference plane |
| $y_i$ | = constant density value of $y$ |
| $y_s$ | = shock coordinate |
| $\Delta y$ | = change in $y$ due to reactions |
| $\Delta y(\eta, z)$ | = conical part of $\Delta y$ |
| $(x_s - y_1)\Delta y(x)$ | = nonconical part of $\Delta y$ |
| $\alpha$ | = degree of dissociation |
| $\beta$ | = angle between surface normal and mainstream |
| $\delta$ | = wedge semivertex angle |
| $\Delta$ | = shock standoff distance |
| $\varepsilon$ | = inverse shock density ratio |
| $\Delta_{cp}$ | = forward center-of-pressure shift |
| $\Theta_d$ | = characteristic temperature for dissociation |
| $\mu$ | = wave angle in shock layer |
| $\xi$ | = binary scaling variable, Eq. (2) |
| $\rho$ | = density |
| $\rho_d$ | = characteristic dissociation density |
| $\rho_s$ | = density at distance $s$ |
| $\sigma_f$ | = frozen reaction length |
| $\phi$ | = angle between shock and mainstream |
| $\Psi$ | = angle between normal to reference plane and mainstream |
| $\omega$ | $= (\rho/\rho_o - 1)$ |
| $\Omega$ | $= (\mathrm{d}\alpha/\mathrm{d}t)_0 a/u_\infty$ |
| $(\mathrm{d}\alpha/\mathrm{d}t)_o$ | = dissociation rate at the shock |

*Subscripts*

| | |
|---|---|
| $b$ | = surface |
| $\infty$ | = upstream |
| 0 | = at the shock |

## Introduction

THE flowfields associated with hypervelocity flight are characterized by the appearance of real-gas effects due to molecular dissociation of air, and these do not always take place with the air in dissociative chemical equilibrium. In fact, dissociative nonequilibrium prevails for substantial regions of the flow about most flight vehicles, and for re-entry gliders in particular, it applies over most of the flowfield.

This may be demonstrated by taking a shock inclined at 40 deg as representative of those preceding most of the flowfield about a re-entry glider, and determining the altitudes and velocities at which chemical freezing or equilibrium, respectively, will occur in distances comparable to a typical vehicle dimension. As shown in Fig. 1, this leads to two boundaries on a velocity-altitude diagram. Above the upper boundary, reactions are so slow that no significant effect takes place within 1 m of the shock, implying that the flow is, in effect, "frozen" and behaves as a perfect gas. Below the lower boundary, reactions are so fast that equilibrium is achieved within 1 m of the shock, and the flow behaves as an equilibrium real gas. The figure shows a typical trajectory for a re-entry glider, and it can be seen that it flies in the nonequilibrium regime between the two boundaries.

This paper deals with nonequilibrium phenomema in inviscid flows, phenomena that influence features such as the shock location upstream of a blunt body or a wing, the inviscid

Received Dec. 29, 1987; presented as Paper 88-0459 at the AIAA 26th Aerospace Sciences Meeting, Jan 11–14, 1988. Reno, NV; revision received Oct. 26, 1988. Copyright © 1989 American Institute of Aeronautics and Astronautics, Inc. All rights reserved.

*Professor, Department of Mechanical Engineering. Member AIAA.

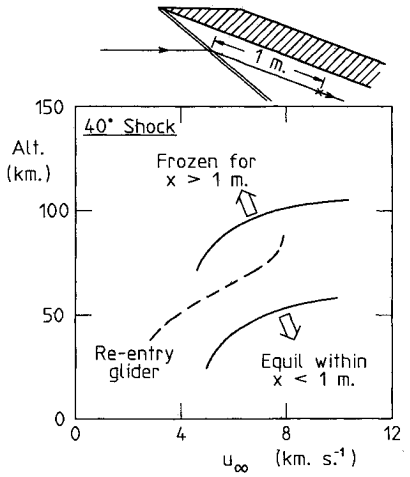


**Fig. 1 Nonequilibrium regime in hypervelocity flight.**

shock detachment on a wedge or in a corner such as a wing root, the density and velocity field far downstream of a blunt nose, and the pitching moment on a lifting surface. Such influences are quantified here by taking an approximate analytical approach, in which the following assumptions are made:

1) Backward reaction rates may be neglected for highly nonequilibrium flows. This is justified by noting that equilibrium is achieved by recombination rates rising to values such that they match the dissociation rates. The ratio between the two rates is directly dependent on the density, which decreases with increasing altitude. Therefore, the wide separation between the frozen and equilibrium boundaries in Fig. 1 implies that dissociation reactions are dominant over most of the nonequilibrium region.

2) The gas may be adequately represented by the Lighthill-Freeman[1] model of an ideal dissociating gas. This model provides a good quantitative representation of nitrogen and oxygen alone and a good qualitative representation of air, even when nitric oxide is formed.

3) Only the flow downstream of a strong shock need be considered, since a strong shock usually will be needed in order to give rise to real-gas effects. The shock could be a bow shock, as for a re-entry glider, or a local shock, as at the leading edge of a fin on a slender acceleration vehicle.

This approximate approach leads to simplified, tractable models that, it is hoped, make the dominant phenomena apparent.

## Analysis

For an ideal dissociating gas, the equation for the rate at which the gas dissociates in passing along a streamline after crossing a shock is written as

$$\frac{d\alpha}{ds} = Cq^{-1}T^{-n}\rho(1-\alpha)\exp(-T^{-1}) \tag{1}$$

Putting

$$\xi = \int_0^s \rho q^{-1}\, ds \tag{2}$$

this becomes

$$\frac{d\alpha}{d\xi} = CT^{-n}(1-\alpha)\exp(-T^{-1}) \tag{3}$$

where, as noted, the recombination term has been neglected. Also, the enthalpy per unit mass of an ideal dissociating gas and the equation of state are written, respectively, as

$$h = D\{(4+\alpha)T + \alpha\} \tag{4}$$

$$p = D\rho T(1+\alpha) \tag{5}$$

Thus, since the stagnation enthalpy $h + 0.5\,q^2$ is constant along streamlines, and the momentum equation is

$$\frac{dp}{d\xi} = -\rho q \frac{dq}{d\xi}$$

it follows that, along streamlines,

$$(4+\alpha)\frac{dT}{d\xi} = -(1+T)\frac{d\alpha}{d\xi} + (\rho D)^{-1}\frac{dp}{d\xi} \tag{6}$$

## Constant-Pressure Flow

If the pressure remains constant along a streamline after a shock, then Eq. (6) becomes

$$(4+\alpha)\frac{dT}{d\xi} = -(1+T)\frac{d\alpha}{d\xi} \tag{7}$$

and combining this with Eq. (3) yields

$$\frac{dT}{d\xi} = -CT^{-n}(1+T)(1-\alpha)(4+\alpha)^{-1}\exp(-T^{-1}) \tag{8}$$

Taking $T \ll 1$, and integrating by parts, Eq. (8) becomes

$$\exp(T^{-1} + 2\ell n\, T) - \exp(T_o^{-1} + 2\ell n\, T_o) = CT^{-n}(1+T)(1-2T)(1-\alpha)(4+\alpha)^{-1}\xi \tag{9}$$

where a term

$$-C\int_{\xi=0}^{\xi} \xi\, d\{T^{-n}(1+T)(1-2T)(1-\alpha)(4+\alpha)^{-1}\}$$

has been neglected because, as shown in Ref. 2, it is only of the order of $T$ in comparison with the left-hand side of Eq. (9).

At normal flight densities, the neglect of $T$ is justified by noting that it is only of the order of $10^{-1}$. However, Eq. (3) indicates that dissociation will take place at any temperature, no matter how low, provided that $\xi$ is large enough. Thus, in principle, $T$ can be made as small as needed in order to make the approximation valid, although it should be understood that the associated physical flow then will be of extremely large scale and that, in order that the assumption of no recombination be valid, the densities will be very low.

Equation (2) is compared with exact numerical solutions in Fig. 2a for some examples with zero dissociation at the shock. In order to ensure that the exact solutions correctly represented the behavior of an ideal dissociating gas for large values of $\xi$, the backward reaction term was included in the rate equation.[1] The equilibrium values of the dissociation fraction, which are achieved for $C\xi$ somewhat in excess of 1000, are also shown on the curves, as an indication of the range of dissociation levels covered. It can be seen that Eq. (9) yields a reasonably accurate estimate of the temperature, particularly at the lower temperatures associated with high values of $C\xi$. Of course, the level of accuracy will deteriorate again at very high values of $C\xi$ as the exact curves approach their equilibrium values, but this does not happen within the range of $C\xi$ covered in Fig. 2a.

There are two features of Fig. 2a that are particularly worth noting. The first is that, over any decade of $\xi$, there is not a large variation in $T$. It must be admitted that it may be

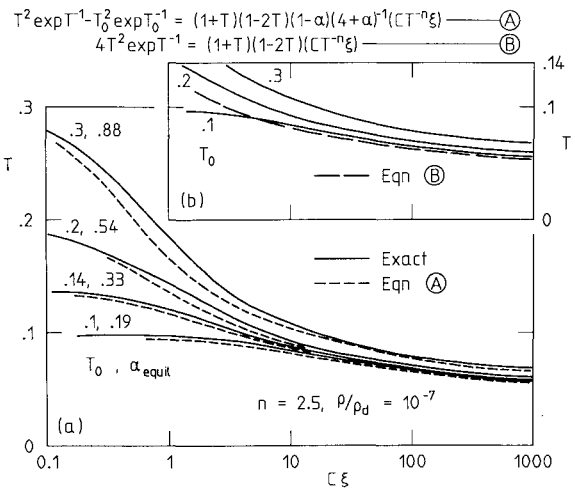


**Fig. 2 Constant-pressure dissociation.**

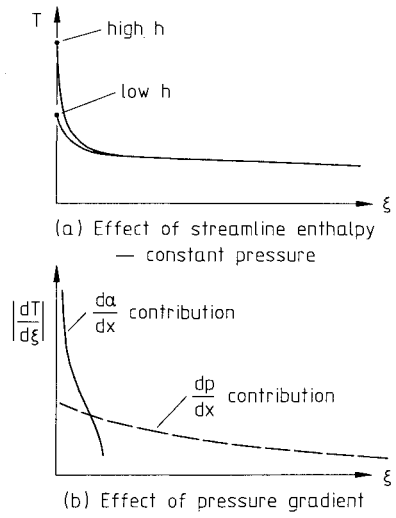


**Fig. 3 Decay of reaction rate.**

necessary to stretch the point somewhat in order to apply it to all of the curve for $T_o = 0.3$, since there are parts of that curve where the variation of $T$ over one decade is as much as 50% of the mean value. However, it is clear that for the lower values of $T$, with which this work is concerned, this is an acceptable statement.

The reason for this effect lies in the strong exponential term in Eq. (8). Because $T$ is small, a small increase in $T$ will cause a strong increase in $dT/d\xi$. Since $T$ decreases monotonically with increasing $\xi$, values of the temperature gradient, $dT/d\xi$, which are large in relation to other values in the zone of interest are only possible close to the shock. Thus, $T$ can only increase significantly near the shock, and therefore it must be approximately constant over most of the distance downstream of the shock.

The second feature is that the curves of Fig. 2a converge as $C\xi$ increases, indicating that $T$ then becomes approximately independent of the temperature at the shock. Because $T \ll 1$, the first term on the left-hand side of the equation rapidly becomes greater than the second term as $T$ falls, and therefore, sufficiently far from the shock, the second term may be neglected. Then, assuming that $\alpha \ll 1$, Eq. (9) becomes

$$4 \exp(T^{-1} + 2 \ell n\, T) = (1 + T)(1 - 2T)CT^{-n}\xi \qquad (10)$$

i.e., $T$ is a function only of $\xi$. Equation (10) is compared with the exact solutions in Fig. 2b. It can be seen that it predicts the temperature very well when the dissociation levels are not too high, but as values of $T_o$ increase, the correspondingly increasing values of $\alpha$ in the region of interest cause Eq. (10) to become increasingly approximate. Thus, Eq. (10) should be used only for values of $\alpha$ that are not too close to unity.

Now, using Eq. (5), $\xi$ can be written as

$$\xi = \int_0^s p\{q(DT(1+\alpha)\}^{-1}\, ds \qquad (11)$$

For the strong hypersonic shocks that are considered here,

$$p \approx \rho_\infty u_\infty^2 \sin^2 \phi$$

$$q \approx u_\infty \cos\phi$$

from which, using the constant-temperature approximation (which also implies constant $\alpha$), Eq (11) becomes

$$\xi = u_\infty \sin\phi \tan\phi\{DT(1+\alpha)\}^{-1}\rho_\infty s \qquad (12)$$

The only factor in this relation that is affected by the streamline enthalpy is the one involving $\alpha$. Now, variation in $(1+\alpha)$ can only change $\xi$ by a factor of 2, and the constant-temperature approximation implies that such a variation has only a weak effect on the value of $T$. Thus, for the purpose of determining $T$, $\xi$ is effectively independent of the streamline enthalpy for any value of $\alpha$. That is, determination of the temperature is decoupled from the thermodynamics of the flow.

This can be compared with perfect-gas flows, where the streamline enthalpy determines the temperature. For nonequilibrium real-gas flows, the binary scaling variable $\xi$ plays that role.

The reason for this can be seen by referring to Fig. 3a. When the streamline enthalpy is raised from one level to a higher one, the temperature at the shock is increased, but by virtue of the exponential term in Eq. (8), the reaction rate is greatly enhanced. This ensures that the temperature falls very rapidly along the streamline and, therefore, that it quickly returns to values associated with the lower enthalpy within a short distance from the shock. Essentially, the reaction processes initially take place at a much higher rate than the flow processes, but the strong exponential term ensures that the reaction rate is driven down until it matches the flow processes.

Each of the constant-temperature approximations and thermodynamic decoupling effects offers a means of making simple approximate calculations of nonequilibrium real-gas flows. Some examples of such calculations follows.

## Constant-Temperature Approximation

### Shock Standoff on a Sphere

The pressure in the shock layer on a sphere varies as $\cos^2\beta$, and therefore the flow sufficiently close to the stagnation point may be regarded as a constant-pressure one. The constant-temperature approximation then implies that the density may be taken to be approximately constant within the shock layer and the shock standoff distance calculated by using the relation for constant-density flow presented in Ref. 3, i.e.,

$$\Delta/a = 0.78\, \rho_\infty/\rho_s \qquad (13)$$

Determination of $\rho_s$ requires determination of $T$, which requires selection of an appropriate value of $\xi$. Since the sonic point at the shock occurs near $\beta = 30$ deg, the arc length corresponding to $\beta = 15$ deg is a suitable value of $s$, whilst the velocity can be taken as the value immediately downstream of the normal shock. Using the density at the shock, a rough estimate of $\xi$ then can be substituted into Eq. (9) and, with $\alpha = \alpha_o$, a preliminary estimate of temperature can be ob-

tained. This can be combined with a new dissociation level, obtained from this temperature and the stagnation streamline enthalpy, and with the Newtonian pressure, to obtain a better estimate of density. If desired, the cycle can be repeated to improve the estimate further, before the final value is then substituted into Eq. (13) to obtain the shock standoff.

Calculations using this method are compared in Fig. 4 with results of computational simulations for dissociating nitrogen. The computations were performed by Hornung[3] and employed a reaction model in which nitrogen molecules and nitrogen atoms were treated separately as dissociation collision partners. The present calculations were performed with $n = 1.5$, predominantly representing the nitrogen molecules, and are seen to produce standoff values that generally are within 10% of the computed values. Lowering the value of $n$ would tend to provide better representation of atoms as collision partners and would produce closer agreement with the computational simulations at the higher values of $\Omega$, where more atoms are present.

## Shock Detachment on a Wedge

As the vertex angle of a two-dimensional wedge is increased, a point is reached at which the shock detaches and, with further increase in the wedge angle, moves upstream of the vertex of the wedge. This effect is sensitive to the shock-layer-to-freestream density ratio and therefore is subject to real-gas effects. Since the detached flowfield tends to be dominated by a strong, approximately normal shock, the subsonic region downstream of that shock approximates to a constant-pressure flow, and the constant-temperature approximation will again apply.

In Fig. 5, calculations of shock detachment for nitrogen are compared with experimental results obtained by Hornung and Smith.[4] The value of $\xi$ for the calculations was obtained by using $u_\infty \cos\delta$ for the shock-layer velocity, putting $s = 0.5\ w = 25$ mm, and taking the density at the shock wave. Then, as in the previous calculations, a brief iteration was used to obtain the shocklayer temperature. Since the shock is normal or nearly normal in the detachment region, the streamline enthalpy was taken as that for a normal shock, and this yielded the dissociation fraction. By referring to the normal shock density ratio, the shock-layer density ratio then could be obtained.

The shock detachment was obtained by using experimental results for argon, obtained at a Mach number of 16, which are also shown in Fig. 5. These results were used to predict nitrogen shock detachment by employing the three-dimensional blunt-body transformations of Ref. 5, i.e., by equating the values of

$$\sqrt{\rho_s/\rho_\infty - 1}\cot\delta \quad \text{and} \quad \sqrt{\rho_s/\rho_\infty - 1}\,\Delta/w$$

respectively, between the two flows.

As seen in the figure, the resulting prediction of shock detachment is close to the experimental values, except near detachment. There, the small scale of the detachment region is expected to change the effective value of $\xi$. Predictions of detachment for a perfect gas with a ratio of specific heats of 1.4 and for an equilibrium real gas also are shown. The nonequilibrium detachment is well removed from either of these two extremes.

## Thermodynamic Decoupling

Equations (10) and (12) have been used to argue that, because $\xi$ is only weakly dependent on the streamline enthalpy, $T$ is independent of the flow thermodynamics. This argument can be carried further by noting, from Eq. (12), that substantial variations in $u_\infty$ and $\phi$ may take place without altering the order of magnitude of $\xi$ and therefore, from Eq. (1), without significantly altering $T$. This implies that the temperature is approximately independent of the shock angle and flight speed.

As a test of this conclusion, some experimental measurements of shock standoff at the midplane of delta wings in air are presented in Fig. 6. While the reactions involving nitric oxide make the chemistry of air somewhat more complicated than that of an ideal dissociating gas, the net dissociation rates at the temperatures of interest in suborbital flight yield effects that are not dissimilar to the dissociation of pure oxygen, and so thermodynamic decoupling of the temperature also is expected for air.

Figure 6a shows the effect of varying the shock angle of incidence of the wing at a fixed stagnation enthalpy.[6] It is seen that when the measured shock standoff at $\beta = 50$ deg is used as a reference condition, the constant-temperature assumption can be used to make a satisfactory prediction of shock standoff at all other values of $\beta$. As a matter of interest, this is compared with the shock standoff variation for a perfect gas, where the shock-layer density, rather than the temperature, is constant, and this is seen to produce a distinctly different result.

Figure 6b shows the effect of varying the flight speed by varying the flow stagnation enthalpy. The constant-temperature curve employed the same reference condition as in Fig. 6a

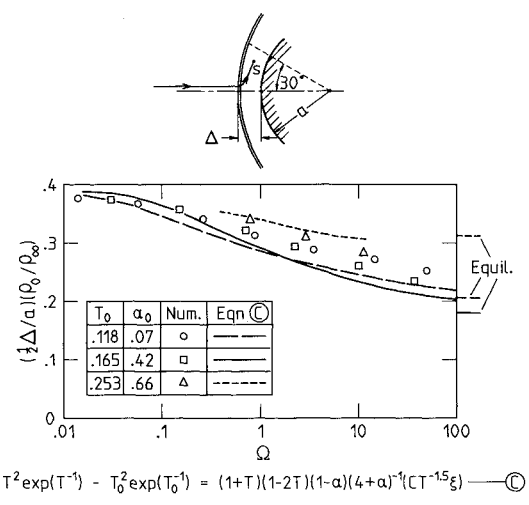


Fig. 4 Standoff distance on sphere.

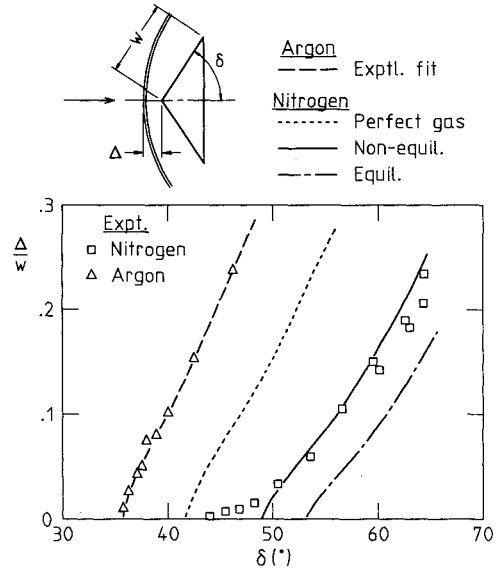


Fig. 5 Shock detachment on a wedge (nitrogen test gas, $u_\infty = 5.5$ km s$^{-1}$, $\rho_\infty = 0.0026$ kg m$^{-3}$, $\alpha_\infty = 0.1$, Mach no. 7.5).

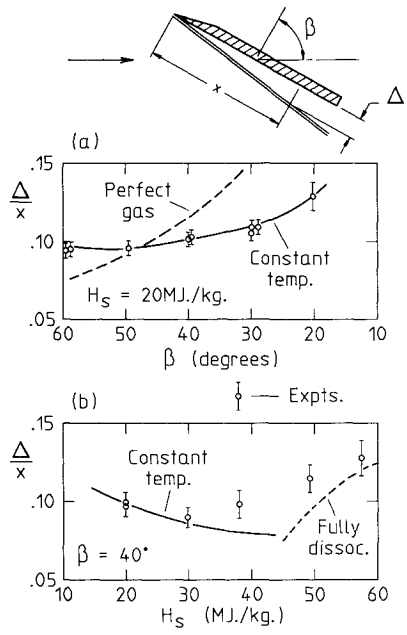


**Fig. 6 Thermodynamic decoupling—shock standoff on flat delta wing ($H_s$ = stagnation enthalpy, leading-edge sweep = 75 deg),**

and is consistent with the experiments at 20 MJ.kg$^{-1}$ and 30 MJ.kg$^{-1}$. At higher enthalpies corresponding to superorbital flight speeds, the gas in the shock layer approaches complete dissociation, and temperatures may be expected to exceed the reference value. This is evident in the experimental shock standoff at 38 MJ.kg$^{-1}$, where constant-temperature calculations indicate that 90% of the air molecules are dissociated. Constant-temperature calculations also indicate complete dissociation at 45 MJ.kg$^{-1}$, and it can be seen that a calculation based on the assumption of complete dissociation tended toward the experiments at the highest stagnation enthalpy tested.

## Flow with Pressure Gradient—Curved Shock

The approximations developed up to this point have been based on the assumption that the last term in Eq. (6), involving the pressure gradient, can be neglected; i.e.,

$$\left|(4+\alpha)\frac{dT}{d\xi}\right| \gg \left|(\rho D)^{-1}\frac{dp}{d\xi}\right|$$

Using Eq. (5), differentiating Eq. (10), and neglecting terms of $\mathcal{O}(T)$ compared with unity, the inequality becomes

$$|4T\xi^{-1}| \gg \left|p^{-1}\frac{dp}{d\xi}\right|$$

implying that a pressure change $|\Delta p|$ over a length corresponding to $\xi$ must be such that

$$|\Delta p|p^{-1} \ll 4T \tag{14}$$

if the pressure gradient is to be negligible.

For the convex curved bow shock that normally is associated with hypervelocity flight, the proportional pressure drop along a streamline is of order unity over the body length, and so the condition of Eq. (14) is not satisfied. However, it then is possible to proceed with another approximation.

Referring again to Eq. (6), it can be seen that for the negative pressure gradient that characterizes the flow after a convex shock, the pressure gradient term on the right-hand side of the equation cooperates with the dissociation term to reduce the temperature. However, the strong exponential factor in the dissociation term ensures that this term is dominant close to the shock. As shown in Fig. 3b, the magnitude of the dissociation term falls rapidly in passing downstream until the contribution of the pressure-gradient term becomes significant. Further cooling then reduces the magnitude of the dissociation term even more and it, in its turn, becomes insignificant. Thus, dissociation effectively ceases, the reaction is "quenched," and the quenched gas exhibits perfect-gas behavior as it passes downstream.

The change from dissociation dominance to a quenched reaction occurs within a small distance along the streamline. This follows from noting that when the pressure gradient becomes significant, Eqs. (5) and (6) imply that

$$T^{-1}\frac{dT}{d\xi} = 0\left(p^{-1}\frac{dp}{d\xi}\right)$$

indicating that only small proportional changes in $p$ are needed to bring about the strong reductions in $\exp(-T^{-1})$ that quench the reaction. Since the proportional pressure gradient has been taken to be of order unity, this implies that the quenching occurs within a small distance along the streamline, i.e., it is "sudden," Moreover, since the proportional pressure gradient is not small, quenching must occur where the proportional temperature gradients are not small and, by the previous discussion of Fig. 3a this can only be close to the shock.

An approximate estimate of the quenching temperature can be obtained by equating the last two terms in Eq. (6) which, when Eqs. (2) and (3) are used and $\alpha$ and terms of $\mathcal{O}(T)$ are neglected in comparison with unity, yields

$$T_Q^{-1} = -\ell n\left\{(C\rho^2 D)^{-1}q\frac{dp}{ds}\right\}$$

Then, remembering that for strong shocks, streamlines tend to follow the shock, and that the pressure is given by the Newtonian formula, it can be deduced that

$$T_Q^{-1} = \ell n\{\rho CR\tan\phi(2u_\infty\cos\phi)^{-1}\} \tag{15}$$

where $\alpha$ and terms of $\mathcal{O}(T)$ are again neglected.

Hornung[7] has performed a more rigorous analysis of the quenching effect and finds that

$$T_Q = \sigma\{1+\sigma\ell n\,\sigma+\sigma\ell n(1+4To)+0(\sigma^2)\} \tag{16}$$

where

$$\sigma^{-1} = \ell n\{(1+\alpha)T^{-n}\rho CR\tan\phi(3u_\infty\cos\phi)^{-1}\}$$

Now, since $C$ is a large constant,[1] it is the dominant term in both Eqs. (15) and (16), and for a strong bow shock without order-of-magnitude variations in the shock radius of curvature, $T_Q$ is approximately constant. Thus, the constant-density ratio strong shock generated in a perfect gas is replaced by a constant-temperature ratio one in a nonequilibrium gas.

Hornung[7] has presented experimental measurements that support the concept of a constant-temperature shock. However, a second aspect of interest is that the quenched gas is expected to expand as a perfect gas as it passes along streamlines, affecting conditions downstream. This is illustrated in Fig. 7, where the results of numerical calculations supplied by Macrossan are presented. These were made by the equilibrium flux method[8] for ideal dissociating gas flow of nitrogen over a 15 deg wedge with a cylindrically blunt nose. As for the higher-density experimental case in Ref. 8, the calculations showed that the dissociation fraction remained approximately constant along any streamline.

As shown in the pressure profile and the pressure contours in Fig. 7a, pressure ratios are approaching the wedge asymptotic value of 50 at the trailing edge. Thus, the profiles of Fig. 7b represent a nearly asymptotic downstream state. They are

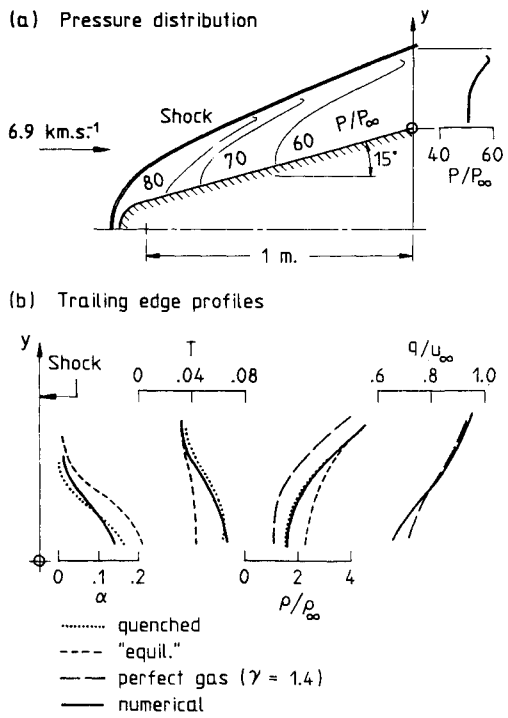


**Fig. 7 Reaction quenching in nitrogen—effect on afterbody flow ($\rho_\infty = 10^{-4}$ kg m$^{-3}$, $\alpha_\infty = 0$, $T_\infty = 252$ K, $r_n = 0.1$ m).**

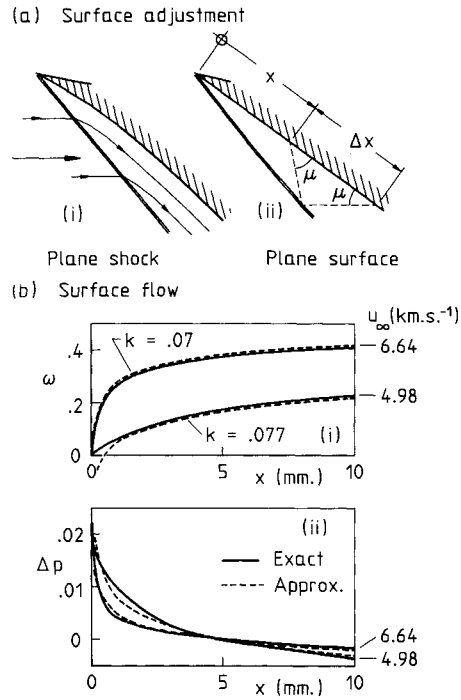


**Fig. 8 Flow over wedge in air (leading-edge shock angle $\phi = 40$ deg, $T_\infty = 273$ K, $P_\infty = 0.01$ atm, $\alpha_\infty = 0$).**

not carried to the surface because the surface streamline passes through an equilibrium region at the stagnation point. In order to indicate the extent of the departure from equilibrium, pseudoequilibrium values of $\alpha$ and $T$ have been obtained by allowing a gas sample to relax to equilibrium without altering its internal energy or density. When these are compared with the calculated profiles, it can be seen that the gas is considerably removed from equilibrium, particularly on the streamlines close to the surface, which have passed through the strongest part of the bow shock. The downstream effect of quenching on fluid dynamic variables is shown in the profiles of $\alpha$, $T$, and $\rho$. The quenched profiles, which are obtained by using Eq. (16) to yield the quench temperature and then expanding as a perfect gas along streamlines downstream of the shock, are seen to agree satisfactorily with the numerical results. For comparison, pseudoequilibrium and perfect-gas profiles of density for the same shock shape and the trailing-edge pressure profile also are shown and are seen to differ substantially from the numerical results. For interest, velocity profiles also are displayed, and they show the increase in vorticity toward the surface that is associated with the dissociation.

## Second-Order Effects—Center of Pressure

By contrast with quenched flows, where the pressure gradient drastically affects the reaction processes, flows also exist in which small pressure changes produce significant effects without modifying the reactions. This is true of flat plates or delta wings at incidence, where reaction-induced pressure changes may be sufficiently small to produce a constant-pressure flow within the meaning of the inequality of Eq. (14) but nevertheless may be large enough to significantly influence the position of the center of pressure. Both cases are considered here, beginning with the simpler, two-dimensional flow represented by an inclined flat plate or wedge.

## Wedge Flow

As explained in Refs. 9 and 10, the reacting flow over a wedge may be described by first considering the flow downstream of a plane oblique shock, as in Fig. 8a. Noting that

$$\rho_\infty/\rho_0 - \rho_\infty/\rho = \varepsilon\omega(1+\omega)^{-1}$$

it can readily be shown that the pressure rise at the curved surface that supports this shock is given by

$$\Delta p_n = \rho_\infty u_\infty^2 \cos^2\phi\ \varepsilon\omega(1+\omega)^{-1} \tag{17}$$

whereas the surface curvature is given in terms of the change in surface angle of incidence with respect to the leading edge angle as

$$\beta_L - \beta = \cot\phi\ \varepsilon\omega(1+\omega)^{-1} \tag{18}$$

where $\beta_L - \beta$ has been written in place of the tangent of that angle, and $\omega$ represents values on the surface.

Then, the body surface can be converted to the plane surface associated with a wedge by applying a change in incidence equal and opposite to that specified by Eq. (18). As shown in Fig. 8 (ii), this produces an expansion originating at the surface, which leads to a curved shock wave and a change in the surface pressure.

Taking a point at a distance $x$ from the leading edge, the expansion propagates along a local Mach line to the shock, where it will reflect with some attenuation and propagate back towards the surface, where it reflects again, and so on. If $\varepsilon_m$ is a mean value of the inverse shock-density ratio for the shock layer, then putting $\mu \approx \sin\mu \approx \tan\mu$, it can be readily shown that $\mu = \sqrt{\gamma\varepsilon_m}\cot\phi$, where $\gamma$ is the frozen ratio of specific heats in the shock layer. Remembering that the distance between the shock wave and the surface at $x$ can be approximated as $\varepsilon_m x \cot\phi$, it follows that $\Delta x$, the downstream distance over which one reflection cycle takes place, is given by

$$\Delta x = 2x\sqrt{\varepsilon_m/\gamma} \tag{19}$$

Following Ref. 6, an approximation for the variation of density along a streamline is introduced by writing

$$s(1+\omega)^{-1}\frac{D\omega}{Ds} = K \tag{20}$$

where $K$ is a constant. For $\omega \ll 1$, expanding $\ell n(1+\omega)$ as a Taylor series allows this expression to lead to the approximation

$$\omega = -K\,\ell n(\sigma_f/x) \tag{21}$$

for the surface streamlines, where $\sigma_f$ is the distance downstream of the shock for which reactions remain frozen.

For dissociating air, $K$ is a small number, of the order of 0.1, implying that an increase in $x$ by, for example, a factor of two leads to only a relatively small change in $\omega$. Referring to Eq. (19), it can be seen that for a vanishingly small $\varepsilon_m$, many wave reflections will take place over the streamwise distance required for this small change, allowing the tangent wedge formula to be used in estimating the change in surface pressure due to surface adjustment. In practice, $\varepsilon_m$ is small enough to allow only a couple of reflections, but a few numerical examples serve to indicate that this is enough to reduce the error in the tangent wedge formula to less than 10%, which is an adequate approximation. Neglecting terms of order $\varepsilon$ in comparison with unity, the tangent wedge formula may be written as

$$\Delta p_t = -\rho_\infty u_\infty^2 \sin 2\phi\,(\beta_L - \beta)$$

or, substituting from Eq. (18), as

$$\Delta p_t = -2\rho_\infty u_\infty^2 \cos^2\phi\,\varepsilon\omega/(1+\omega) \tag{22}$$

Combining this with Eq. (17), the resultant pressure change due to reactions at the surface of the wedge becomes

$$\Delta p = -\rho_\infty u_\infty^2 \cos^2\phi\,\varepsilon\omega/(1+\omega) \tag{23}$$

In Fig. 8b, this is compared with the results of calculations made by the method of characteristics.[11] Figure 8b (i) shows density distributions after the plane shock[12] of Fig. 8a (i), and it is seen that the relation of Eq. (21) yields a good approximation for the higher velocity but is less satisfactory for the lower velocity at small values of $x$. This is because the reaction develops more slowly in that case, and the transition from zero reaction to Eq. (21) requires a larger distance. The influence of this effect is seen in Fig. 8b (ii), where the pressure distributions corresponding to the plane surface is Fig. 8a (ii) are displayed. It can be seen that the approximate surface pressure, calculated according to Eq. (23), agrees more closely with exact surface pressures for the higher than for the lower velocity. But in both cases, Eq. (23) is sufficiently accurate to use in calculating the center-of-pressure shift.

In the absence of reactions, the center of pressure is located at the midchord point. Thus, the forward shift due to reactions can be estimated by writing down the clockwise, "nose-up" pitching moment about midchord due to $\Delta p$. Then, substituting from Eq. (23), neglecting $\omega$ in the denominator of $\Delta p$, integrating, and dividing by the Newtonian normal force $\rho_\infty u_\infty^2 \ell \cos^2\phi$, it is found that

$$\Delta_{cp} = \varepsilon KL/4 \tag{24}$$

It might be noted that this simple relation comes about because it has been possible to use the tangent wedge approximation to relate pressure changes to corrections to the reaction-induced surface slope, and this is only possible because the reaction-induced surface slope changes most rapidly near the leading edge, i.e., close to the shock wave. Thus, this can be seen as another manifestation of the mechanism that allows the constant temperature approximation and is discussed in the paragraphs following Eq. (9).

## Delta Wings

For a zero-yaw delta wing of sufficiently high aspect ratio at a sufficiently low angle of incidence, the leading edge is supersonic and the spanwise velocity component on the wing surface is small. The strip theory approximation[13] then allows the flow in any streamwise plane to be treated as two-dimensional and independent of the flow in other streamwise planes. Under such conditions, the analysis developed for wedge flow can be applied to the delta wing, and this leads to a center-of-pressure shift given by

$$\Delta_{cp} = \varepsilon K\ell/6 \tag{25}$$

However, at low to medium aspect ratios and sufficiently high angles of incidence, the leading edge is subsonic and, except at the vertex, the shock wave detaches from the leading edge. Also, spanwise velocity components become too large to be neglected in an analysis of the shock-layer flow. It has been found that not only are such flows conical in nature when the density is constant in the shock layer[14] but also that the essential conical character is retained for nonequilibrium reacting flow within the shock layer[6] provided that the density variation of Eq. (20) can be used. Of course, the flow is not strictly conical in the latter case, because the average density in the shock layer increases with distance downstream, but it can be accommodated within the framework of a conical analysis by taking a strictly conical shock wave and allowing the surface of the wing to develop curvature, or camber, in the streamwise direction,[6,15] This is shown in Fig. 9a.

The coordinate system for this conical flow analysis is derived from the Cartesian coordinates $x^*$, $y^*$, and $z^*$ shown in Fig. 9a,[14] where $x^*$ and $z^*$ are streamwise and spanwise coordinates, respectively, in a reference plane located close to the wing surface and $y^*$ is the coordinate directed away from the wing. Corresponding velocity components are $u^*$, $w^*$, and $v^*$. The transformations

$$\left.\begin{aligned} &x = x^*/\ell,\ y = y^*/(x^*\varepsilon\cot\psi)\\ &z = z^*/x^*\varepsilon^{1/2}\cot\psi)\\ &u = (u^*/u_\infty - \sin\psi)/(\varepsilon\cos\psi\cot\psi)\\ &w = w^*/(u_\infty\varepsilon^{1/2}\cos\psi)\\ &p = (p^* - p_\infty^*)/(\varepsilon\rho_\infty u_\infty^2\cos^2\psi) - 1/\varepsilon\\ &\rho = \rho_\infty(1+\omega)/\varepsilon \end{aligned}\right\} \tag{26}$$

are used,[6] where $p^*$ and $p_\infty^*$ now are employed to represent the shock layer and freestream pressures, respectively. In addition, an independent conical variable $\eta$ is introduced to identify all streamlines that originate at the shock wave on a given ray through the wing apex. Thus, $y$ becomes a dependent variable, denoting the distance of these streamlines from the reference plane. As indicated in Fig. 9b, the value of $\eta$ is chosen as the value of $z$ on the given ray at the shock wave.

In Ref. 6, these transformations have been used in an analysis to obtain changes in crossflow patterns and shock position that arise from the nonequilibrium reactions. Using Eqs. (12) and (8c) of Ref. 6 and assuming that $\omega \ll 1$, it can be shown that the change in $y$ due to reactions is given by

$$\Delta y = -(y_s - y_i)\,\Delta y(x) - \Delta y(\eta,z) \tag{27}$$

where

$$\Delta y(x) = K\,\ell n[\sigma_f^1/(1-\sigma_f^1)] \tag{28}$$

where $\sigma_f^1 = \sigma_f/x^*$, and $y_s - y_i$, which is a function only of $y$ and $z$, can be obtained from Eq. (12) of Ref. 6 by setting the exponential term in that equation equal to unity. The second

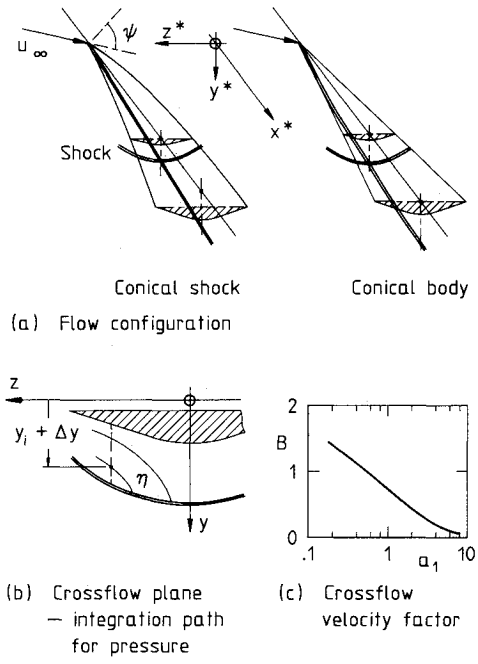


**Fig. 9 Delta-wing flow.**

term on the right-hand side of Eq. (27) contributes only conical terms to $\Delta y$, and hence the nonconical "$x$" dependence is contained in the first term. Since the wing is flat in constant-density flow, the camber of the wing is determined only by this first term, therefore, it can be expressed in terms of the change of the "$y$" coordinate of the surface as

$$\Delta y_{bn} = -K\ell n\,\sigma_f^1\,(y_s - y_i)_b \tag{29}$$

where it has been assumed that reactions are sufficiently developed within the shock layer to put $\sigma_f^1 \ll 1$ and a term of the order of $\sigma_f^1$ has been neglected. Because $\omega \ll 1$, it follows that $\Delta y(x)$, $\Delta y,z)$, and $\Delta y_{bn}$ are $\ll y_i$.

In order to obtain the pressure at the surface, it is first noted that, by following the derivation of Eq. (4.5) in Ref. 15 with the effects of variable density included, the momentum balance in the "$y$" direction may be expressed as a differential equation for the pressure. Thus,

$$(1+\omega)^{-1}\frac{\partial p}{\partial \eta} + (w-z)\left(\frac{\partial y}{\partial \eta}\right)\left(\frac{\partial v}{\partial z}\right) + x\left(\frac{\partial y}{\partial \eta}\right)\left(\frac{\partial v}{\partial x}\right) = 0 \tag{30}$$

A compatibility relation, Eq. (4.7) of Ref. 15, can be used to eliminate $v$ in this equation, and then, remembering that $\omega$, $K$, and $\sigma_f^1$ are all $\ll 1$, and neglecting all terms that involve the product of two small quantities in comparison with those involving only one small quantity, it is found that the nonconical part of the reaction-induced pressure change is given by

$$\Delta p_n = K\ell n\,\sigma_f^1 \int_{\eta_b}^{z} [w(\eta_1) - z]^3 [w(\eta_1) - \eta_1]^{-2} \left(\frac{\partial^2 y_s}{\partial z^2} - \frac{\partial^2 y_i}{\partial z^2}\right) d\eta_1 \tag{31}$$

where $\eta_b$ is the value of $\eta$ at the surface.

As for the case of the wedge, the camber of the wing now can be eliminated by applying a displacement to the surface and the shock that is opposite to that given in Eq. (29). As noted in Ref. 6, this does not change the flow between the shock and the surface, and so the pressure at the surface is affected only through the change in pressure at the shock wave. This pressure is given by Eq. (4.9) of Ref. 15, and using this, it can be shown that the change in $P_o$ as a result of a change of $-\Delta y_{bn}$ in $y_s$ can be written as

$$\Delta p_t = -2\,\Delta y_{bn} - 2x\,\frac{\partial(\Delta y_{bn})}{\partial x}$$

Substituting from Eq. (29) and neglecting a conical term that arises, this becomes

$$\Delta p_t = 2\,K(\ell n \sigma_f^1)(y_s - y_i)_b \tag{32}$$

Adding Eqs. (31) and (32) and substituting for $(y_s - y_i)_b$ by using Eq. (12) of Ref. 6 then yields the part of the reaction-induced change in pressure distribution that will cause a shift in the center of pressure on an uncambered conical wing.

As an example, wings which $w(\eta) = a_1\eta$ are considered, where $a_1$ is a constant. This simple relation provides a reasonable approximation to the shock shape when there is a strong spanwise component to the shock-layer flow, such as occurs for low aspect ratio wings or for wings with a convex cross section,[6,16] as for "diamond" ones. When it is substituted into Eqs. (31) and (32) and the integrations are completed by noting from Eq. (10) of Ref. 6 that $a_1\eta_b = z$, it is found that the two contributions to the pressure at the surface are

$$\Delta p_n = -B_1 K\ell n\,\sigma_f^1$$

where

$$B_1 = a(a_1 - 1)^{-4}(0.5a_1^3 - 3a_1^2 + 1.5a_1 + 3a_1\ell n a_1 + 1) \tag{33}$$

and

$$\Delta p_t = B_2 K\ell n \sigma_f^1$$

where

$$B_2 = 2(a_1 - 1)^{-2}(a_1\ell n a_1 + 1 - a_1) \tag{34}$$

Now, the conical components of the distribution of pressure at the wing surface lead to a center of pressure that is distance $2\ell/3$ from the vortex. Taking the nose-up pitching moment of the nonconical component of pressure about the conical center of pressure and using the transformation of Eq. (26), the pitching moment can be written as

$$\Delta M = -2\ell^3\varepsilon^{3/2}\rho_\infty u_\infty^2 \cos^2\psi\,\cot\psi \int_0^1 \int_0^\Omega [x - 2/3]x(\Delta p_n + \Delta p_t)\,dz\,dx \tag{35}$$

where $z_1^*$ is the semiwidth of the wing at $x^*$ and $\Omega = z^*/(x^*\varepsilon^{1/2}\cot\psi)$. Dividing Eq. (35) by $\rho_\infty u_\infty^2 \cos^2\psi$, the Newtonian pressure, and the planform area of the wing then yields the forward shift in the center of pressure as

$$\Delta_{cp} = \varepsilon K B\ell/9 \tag{36}$$

where

$$B = B_1 - B_2 \tag{37}$$

In Fig. 9c, $B$ is plotted against $a_1$. At relatively low values of $a_1$, Eq. (36) predicts a forward center-of-pressure shift that is about half that obtained on a wedge [Eq. (24)]. As $a_1$ is increased, corresponding to an increase in the spanwise flow component, $\Delta_{cp}$ is reduced. Thus, very slender wings with a cross section convex in the windward direction will experience less centre-of-pressure shift than a flat, only moderately slender wing or a caret wing. Also, provided that $K$ does not change, an increase in the angle of incidence of a given wing will reduce the center-of-pressure shift.

The magnitude of the center-of-pressure shift predicted by Eq. (36) is small, but not insignificant. For example, for a

wing with a 70-deg leading-edge sweep at a flight velocity of 7 km/s and an incidence of $\phi = 50$ deg, appropriate values of $\varepsilon$ and $K$ are 0.16 and 0.14[12] with $a_1 = 0.5$,[6] and this yields a forward shift in the center of pressure of 0.25% of the centerline chord length. It is interesting that the forward shift of the center of pressure experienced by the Shuttle Orbiter on its first flight was approximately 0.75% of the chord length of the vehicle. This indicates that, although the nonequilibrium phenomenon investigated here cannot account for all of the center-of-pressure shift that occurred, it can make a significant contribution.

## Conclusion

In an analysis of the hypersonic flow of a Lighthill-Freeman ideal dissociating gas, the small magnitude of the reduced temperature has been exploited to emphasize the dominance of the exponential term in the expression for the forward reaction rate. This has made it possible to develop approximate concepts that identify the dominant nonequilibrium effects for some significant flow configurations.

For nearly constant-pressure flow, a constant-temperature approximation may be used in which the temperature is taken as constant at a value determined by $\xi$ over most of the nonequilibrium region. This approximation is seen to be effective in predicting the shock standoff on a sphere.

It follows from this constant-temperature approximation that all blunt body flows are essentially constant-density ones, whether they be perfect-gas, nonequilibrium, or equilibrium flows. This is illustrated by using perfect-gas results with argon to predict the nonequilibrium shock detachment distance on a wedge in nitrogen.

Again, in a nearly constant-pressure shock layer, the thermodynamic decoupling of the temperature from the streamline enthalpy allows the temperature to be independent of flight speed and incidence. This is seen to satisfactorily predict the variation of shock standoff with incidence on a delta wing in air. It also is consistent with the variation of shock standoff with stagnation enthalpy, and thus flight speed, provided that the air in the shock layer does not approach complete dissociation.

For a curved bow shock, the downstream pressure gradient causes a reaction-quenching effect leading to a constant-temperature-ratio shock wave, followed downstream by perfect-gas behavior along streamlines. This is confirmed by a numerical simulation of the flow over a blunt wedge.

A second-order theory for nearly constant-pressure flows, which uses the mechanism underlying the constant-temperature approximation, is put forward and is seen to predict satisfactorily the pressure changes caused by reactions on a wedge. The theory is extended to predict the reaction-induced center-of-pressure shift on delta wings. It is found that this is sufficient to make a significant contribution to the center-of-pressure shift experienced on the Space Shuttle Orbiter during its first re-entry.

These approximations are based upon an analysis for an ideal dissociating gas. A similar, if more complicated, analysis could be conducted for air and would be expected to lead to similar approximations.

## Acknowledgment

Much of this work was made possible by the continuing support of the Australian Research Grants Scheme.

## References

[1]Freeman, N. C., "Non-equilibrium Flow of an Ideal Dissociating Gas," *Journal of Fluid Mechanics*, Vol. 4, Pt. 3, 1958, pp. 407–425.

[2]Stalker, R. J., "Post-shock Non-equilibrium Flows in Hypervelocity Aerodynamics," AIAA Paper 88-0459, 1988.

[3]Hornung, H. G., "Non-equilibrium Dissociating Nitrogen Flow over Spheres and Circular Cylinders," *Journal of Fluid Mechanics*, Vol. 53, Pt. 1, 1972, 149–176.

[4]Hornung, H. G. and Smith, G. H., "The Influence of Relaxation on Shock Detachment," *Journal of Fluid Mechanics*, Vol. 93, Pt. 2, 1979, pp. 225–239.

[5]Stalker, R. J., "A Similarity Transformation for Blunt-Body Flows," AIAA Paper 86-0125, Jan. 1986.

[6]Stalker, R. J., "Non-equilibrium Flow over Delta Wings with Detached Shock Waves," *AIAA Journal*, Vol. 20, Dec. 1982, pp. 1633–1639.

[7]Hornung, H. G., "Non-equilibrium Ideal Gas Dissociation after a Curved Shock Wave," *Journal of Fluid Mechanics*, Vol. 74, Pt. 1, 1976, pp. 143–159.

[8]Macrossan, M. N. and Stalker, R. J., "Afterbody Flow of a Dissociation Gas Downstream of a Blunt Nose," AIAA Paper 87-0407, Jan. 1987.

[9]Chong-Wei, C., "Equivalence of Non-equilibrium Flows Behind Normal and Oblique Shock Waves," *AIAA Journal*, Vol. 2, Oct. 1964, p. 1833.

[10]Vincenti, W. G. and Kruger, C. H., *Introduction to Physical Gas Dynamics*, 1st ed., Wiley, New York, 1965, pp. 305–307.

[11]Spurk, J. H., Gerber, N., and Sedney, R., "Characteristic Calculation of Flowfields with Chemical Reactions," *AIAA Journal*, Vol. 4, Jan. 1966, pp. 30–37.

[12]Wittliff, C. E., Sundaram, T. R., Rae, W. J., and Lordi, J. A., "Study of High-Density Hypervelocity Flows and Simulitudes," Arnold Engineering Development Center, Arnold AFB, Rept. AEDC-TR-67-72, April 1967.

[13]Hayes, W. D. and Probstein, R. F., *Hypersonic Flow Theory*, 1st ed., Academic, New York, 1959, pp. 44–47.

[14]Messiter, A. F., "Lift of Slender Delta Wings According to Newtonian Theory," *AIAA Journal*, Vol. 1, April 1963, pp. 794–801.

[15]Hillier, R., "Three-Dimensional Wings in Hypersonic Flow," *Journal of Fluid Mechanics*, Vol. 54, July 1972, pp. 305–337.

[16]Squire, L. C., "Calculated Pressure Distributions and Shock Shapes on Thick Conical Wings at High Supersonic Speeds," *Aeronautical Quarterly*, Vol. 18, May 1967, pp. 185–205.